Precise Speed Estimation From a Low-Resolution Encoder by Dual-Sampling-Rate Observer

Lilit Kovudhikulrungsri, *Member, IEEE*, and Takafumi Koseki, *Member, IEEE*

***Abstract*—This paper describes an effective way to estimate state variables, such as motor speed and disturbance from a low-resolution encoder at low speed by using the dual-sampling-rate observer. The dual-sampling-rate observer estimates the state variables at every DSP control period and correct the estimation error at the instant that the measurement signal is detected. A novel pole assignment method, which considers the relation of the estimation- and error correction periods, is proposed to maintain the stability for long error correcting period. Moreover, the dual-sampling-rate observer can be applied for higher order systems since it is generalized in state space. The effectiveness of the observer is verified through various simulations and experiments.**

***Index Terms*—Digital observer, estimation, intersample, stability, variable sampling rates.**

I. Introduction

LOW-resolution encoders are widely used for traction systems such as rolling stocks, electric vehicles, etc. For example, pulse generators used as speed sensors in Japanese commuter trains have only 60 pulses per revolution (ppr). The accuracy remarkably degrades at low speed, where the encoder pulses cannot be detected at every control period.

The conventional method to obtain the speed is called the numerical difference method. This method is implemented by measuring the change in angle by counting the pulses produced in a counting period and dividing by the counting period. The resolution will be very coarse in case of a small pulse counting period. Hence, this method is not applicable to a low-resolution encoder of which the pulses are not frequently produced.

An alternative way to raise the resolution is to count the time interval between two consecutive pulses [1]. The resolution at low speed is improved, since the interval between two consecutive pulses is relatively long. Conversely, this method has a limitation at high speed. Even though the resolution at low speed is raised, the time delay is unavoidable, since the calculated speed is the average value of the previous interval.

Combination of these methods is proposed by Ohmae *et al.* [2]. This method maintains the resolution by combining the advantages of each method. However, the problem of time delay is still unavoidable.

To avoid this problem, it is necessary to estimate the speed between two consecutive pulses. A powerful method to grasp the speed between the encoder pulses is the "instantaneous speed observer" [3]–[6]. It is a specific discrete-time observer estimating or predicting the speed based on the plant model, which is the mechanical dynamics of a motor, at every control period and correcting the error of estimation when the next pulse is detected. It has been recently applied in the field of traction control of an electric vehicle [5] and rolling stock control [7]–[9]. One of the difficulties in traction control is that it deals with a wide range of speeds. The observer gains were tuned by simply considering only the relation of pole locations on s- and z-planes [4], [8]–[10]. As a result, the system can operate stably in a wide range of speed except at extremely low speed, where pulses cannot be detected frequently. Improvement of the speed estimation can be done by careful consideration of the pulse detection timing [6]. However, the stability issue of the observer is not clarified.

The instantaneous speed observer can be categorized as a multirate sampling observer, since the error-correction period is longer than the estimation period. The multirate sampling theory [11]–[13] has been applied in industrial application such as position control of hard disk drive [14] where the sampling period of plant output is restricted to be relatively longer than the control period of plant input. This method, however, deals with a constant ratio of sampling times. It is different from the instantaneous speed observer where the error correction period varies with the motor speed.

In order to analyze the instantaneous speed of the observer [15], the concept of multirate sampling theory [11]–[14] is applied by taking into account the variation of the ratio of the sampling periods. The stability in ultralow-speed range can be maintained by careful consideration of the relation of estimation- and error correction period. Gain calculation, however, is quite complicated since it needs gain recalculation to stabilize the observer in ultra low speed range.

The observers mentioned in [3]–[9], [15] are the predicting observers, which used the detected output of the previous sampling instant to correct the estimation error. This means that the estimation is likely to be less accurate than correction by the current detected output. The observer that uses the current detected output to correct the estimation error is defined as the current observer [16]. By rearranging the instantaneous speed of the observer based on the current observer; the authors find out a more simple gain calculation that still maintains the performance of the observer.

In this paper, the instantaneous speed observer in state space is generalized. Since it has two sampling periods: error correction period T_1 and the estimation period T_2 it can be defined as "dual-sampling-rate observer." Its principle is introduced in Section III. Derivation and pole assignment of the predicting dual-sampling-rate observer, the gain calculation of which

Manuscript received October 31, 2005; revised February 27, 2006. Recommended by Technical Editor Y. Hori.

L. Kovudhikulrungsri is with Nippon Seiko Kabushiki Kaisha (NSK Ltd.), Tokyo 141-8560, Japan (e-mail: lilit@george24.com; lilit@nsk.com).

T. Koseki is with the Department of Information and Communication, University of Tokyo, Tokyo 113-0033, Japan (e-mail: koseki@koseki.t.u-tokyo. ac.jp).

Digital Object Identifier 10.1109/TMECH.2006.886194

TABLE I
LIST OF SYMBOLS

Symbol	Description
$\mathbf{A}$	Coefficient matrix a state vector
$\mathbf{B}$	Coefficient matrix a input vector
$\mathbf{C}$	Coefficient matrix a output vector
J	Moment of inertia
$\mathbf{L}$	Conventional observer's gain matrix
$\mathbf{L}^*$	Dual-sampling-rate observer's gain matrix
N	Amount of sampling instants in a sampling frame or last sampling instant a sampling frame
T_{1_actual}	Actual interval between two consecutive pulses
T_1	Interval between two consecutive pulses read by the DSP
T_2	Control period
T_L	Load torque
T_m	Motor torque
c	Friction, viscosity of the damper
$\mathbf{e}$	Estimation error vector
g_r	Gear ratio
k	Spring constant
m	Index number of the pulse or sampling frame
n	Sampling instant in a sampling frame
q	Number of poles of the observer
u or $\mathbf{u}$	Input or input vector
x or $\mathbf{x}$	State variable or state vector
$\hat{\mathbf{x}}$	Estimated or corrected state vector
$\tilde{\mathbf{x}}$	Predicted state vector
y or $\mathbf{y}$	Measurement output or measurement output vector
z	Pole on z-plane
θ	Shaft angle or motor angle
ω	Motor angular speed

TABLE II
LIST OF SUBSCRIPTS

Subscript	Description
1	Sampled by T_1
2	Sampled by T_2
3	Third order
5	Fifth order
D	Drive disk's quantity
L	Load disk's quantity
c	Current type observer
cd	Continuous-time with disturbance consideration
i	Index number
p	Predicting type observer

is complicated, is reviewed in Section IV. The current dual-sampling-rate observer which simplifies the gain calculation is described in Section V. The gain calculating procedures of both observers are reported in Section VI. The effectiveness of the observers is verified through various simulations and experiments in Section VII.

II. LIST OF SYMBOLS

The symbols used in this paper and their descriptions are described in Tables I and II.

III. PRINCIPLE OF THE DUAL-SAMPLING-RATE OBSERVER

The principle of the dual-sampling-rate observer is to predict the state variables at every sampling time based on the angle when the pulse is detected and correct the error when the next encoder's pulse is detected.Fig. 1(a) shows a timing diagram of the output of an incremental encoder and the angle detected by the dual-sampling-rate observer. T_{1_actual}, T_1, and T_2 denote

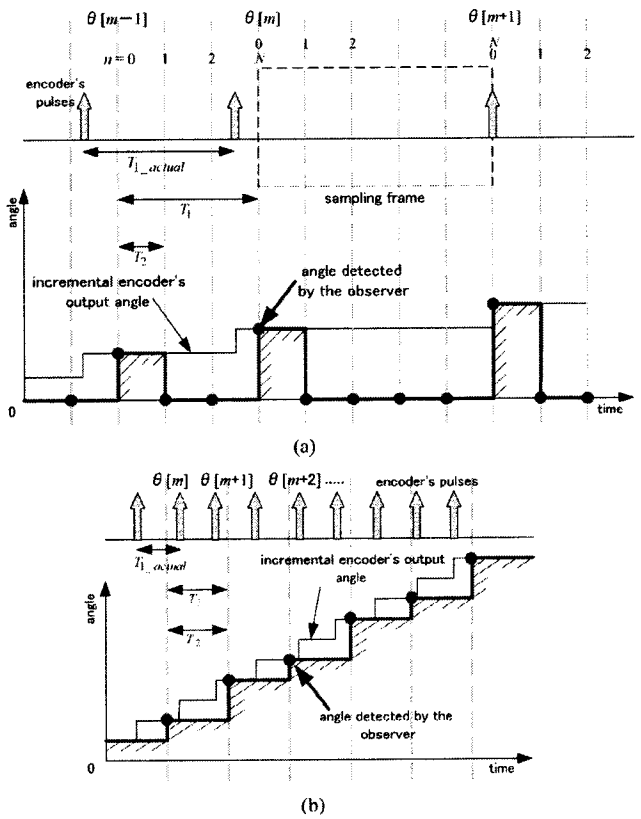

Fig. 1. Timing diagram of the dual-sampling-rate observer when: (a) The period between two consecutive pulses is (a) larger and (b) smaller than DSP control period.

the actual interval between two consecutive pulses, the interval between two consecutive pulses read by the DSP and the control period, respectively. Bold arrows stand for pulses generated by the encoder. It is seen from the figure that the incremental encoder output angle is instantaneously updated when a pulse is detected. This signal is, however, read at the next sampling instant. Therefore, there occurs unavoidable delay. This signal is held for one control period and then reset to zero based on the principle of the observer.

Next, let us consider the case when the motor starts acceleration. The encoder generates the pulses more frequentlywhen the interval between two consecutive pulses that the DSP reads becomes smaller than the control period the pulses can be detected at every control period. In this case, T_1 is equal to T_2 as shown in Fig. 1(b). As a result, the dual-sampling-rate observer predicts and corrects the error at every sampling instant. Therefore, we can conclude that the dual-sampling-rate observer becomes an ordinary discrete-time observer when the interval between two consecutive pulses is smaller than the control period.

The dual-sampling-rate observer can be separated into two types according to the structure: the predicting type that uses the encoder pulse, i.e., the measurement signal, to correct the next state, and the current type, that uses the current measurement signal to correct the current state. Their signal and block diagrams are shown in Fig. 2. The variables $\hat{\mathbf{x}}$, $\tilde{\mathbf{x}}$, $\mathbf{u}$, and $\mathbf{y}$ denote the estimated or corrected state, the predicted state, the input

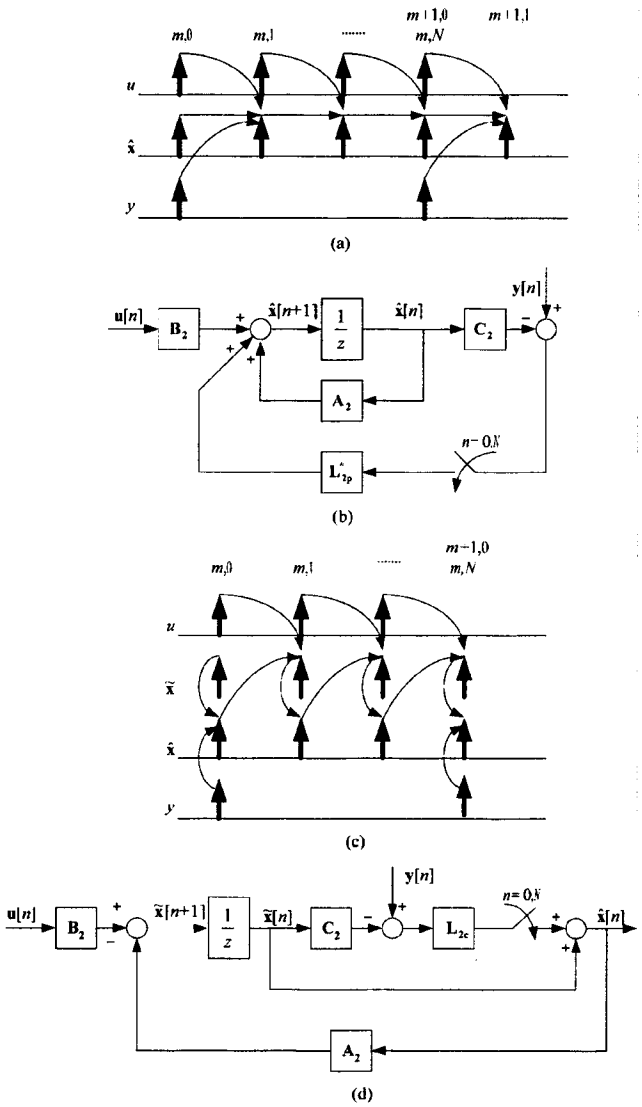

Fig. 2. (a) Signal diagram and (b) block diagram of the predicting type. (c) Signal diagram and (d) block diagram of current type.

and the measurement vectors, respectively. $\mathbf{A}_2, \mathbf{B}_2, \mathbf{C}_2, \mathbf{L}^*_{2p}$, $\mathbf{L}^*_{2c}$ denote the matrices in discrete-time domain sampled by T_2. The subscript 2 indicates that the constant control period T_2 is used as the sampling time. The subscripts p and c denote predicting and current types, respectively.

IV. Predicting Dual-Sampling-Rate Observer

A. Derivation

According to Fig. 1(a), the sampling instant $[m, n]$ is defined by

$$t = mT_1(\theta[m]) + nT_2 = [m, n] \tag{1}$$

where $\theta[m]$, m, and n denote the shaft angle, the index number of the pulses, and the sampling instant the counting of which starts when a pulse is detected and reset when the next pulse is detected, respectively. The value of n is between 0 and N, where N denotes last sampling instant. The relationship between the sampling indices m and n can be concluded as

$$[m, N] = [m + 1, 0]. \tag{2}$$

It is also convenient to define an interval between two consecutive pulses as a "sampling frame." Thus, (2) implies that the N th sampling instant of the current sampling frame is the zeroth sampling instant of the next sampling frame and m is the index number of the sampling frame.

According to the signal diagram in Fig. 2(a), when an encoder pulse is detected, the error of estimation is corrected. On the other hand, when pulses are not detected, the observer principally works as a simulator, predicting the state variables based on the plant model as shown in (3) at the bottom of the page, where $\mathbf{A}_2, \mathbf{B}_2, \mathbf{C}_2$, and $\mathbf{L}^*_{2p}$ denote matrices in discrete-time domain sampled by T_2. The subscript 2 indicates that the constant control period T_2 is used as the sampling time. It is very important to note that the disturbance is included in the state vector for accurate estimation. The block diagram of the predicting dual-sampling-rate observer is shown in Fig. 2(b). Rearranging (3) based on the sampling instant $n = 0$, the state variable can be expressed as

$$\begin{aligned}\hat{\mathbf{x}}[n] = \mathbf{A}_2^n\hat{x}[0] + \mathbf{A}_2^{n-1}\mathbf{B}_2\mathbf{u}[1] + \mathbf{A}_2^{n-2}\mathbf{B}_2\mathbf{u}[0] + \cdots \\ + \mathbf{A}_2^0\mathbf{B}_2\mathbf{u}[n-1] + \mathbf{A}_2^{n-1}\mathbf{L}^*_{2p}(\mathbf{y}[0] - \hat{\mathbf{y}}[0]).\end{aligned} \tag{4}$$

B. Pole Assignment

Pole assignment is achieved by a consideration of the error dynamics of the observer. To do this, it is necessary to rearrange the state vector of the plant in terms of the last-sampling-instant state vector of the previous sampling frame as

$$\begin{aligned}\mathbf{x}[n] = \mathbf{A}_2^n\mathbf{x}[0] + \mathbf{A}_2^{n-1}\mathbf{B}_2\mathbf{u}[0] + \mathbf{A}_2^{n-2}\mathbf{B}_2\mathbf{u}[1] \\ + \cdots + \mathbf{A}_2^0\mathbf{B}_2\mathbf{u}[n-1].\end{aligned} \tag{5}$$

At the instant when the next pulse is detected, i.e., $n = N$, substracting (5) from (4) and using the relation (2), the error of estimation $\mathbf{e}$ of a sampling frame can be expressed as

$$\mathbf{e}[m+1] = \left(\mathbf{A}_2^N - \mathbf{A}_2^{N-1}\mathbf{L}^*_{2p}\mathbf{C}_2\right)\mathbf{e}[m]. \tag{6}$$

Consequently, the observer gains are obtained by placing the poles in the unit circle and solving the equation

$$\prod_{i=1}^{q}(z - z_i) = \left|z\mathbf{I} - \mathbf{A}_2^{N-1}(\mathbf{A}_2 - \mathbf{L}^*_{2p}\mathbf{C}_2)\right| \tag{7}$$

where z_i and q denotes the i th pole on z-plane and the number of poles, respectively.

$$\hat{\mathbf{x}}[n+1] = \begin{cases}\mathbf{A}_2\hat{\mathbf{x}}[n] + \mathbf{B}_2\mathbf{u}[n] + \mathbf{L}^*_{2p}(\mathbf{y}[n] - \mathbf{C}_2\hat{\mathbf{x}}[n]), & n = 0 \\ \mathbf{A}_2\hat{\mathbf{x}}[n] + \mathbf{B}_2\mathbf{u}[n], & n = 1, 2, \ldots, N-1\end{cases} \tag{3}$$

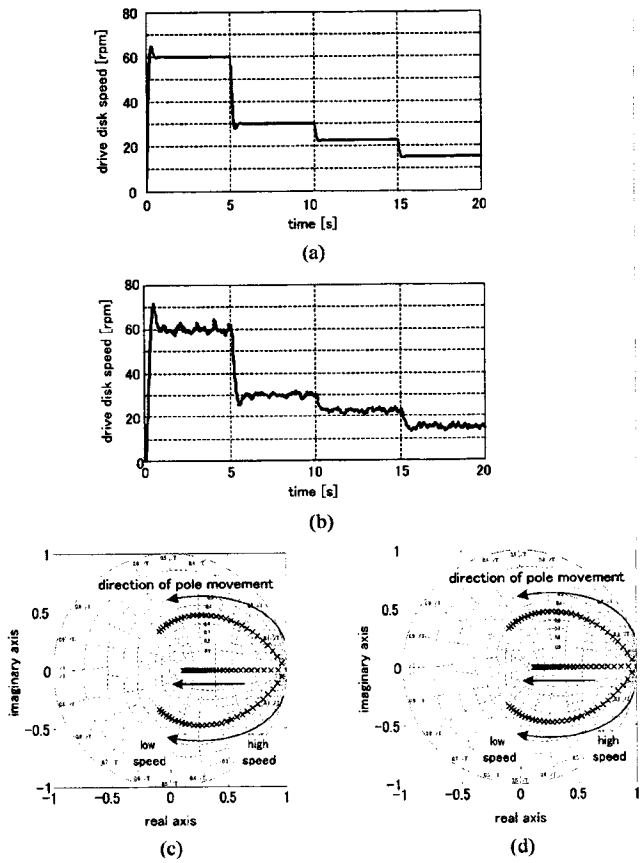

Fig. 3. (a) Simulation and (b) experimental results of the proposed pole assignment. (c) Movement of the poles in design. (d) Actual movement of the poles.

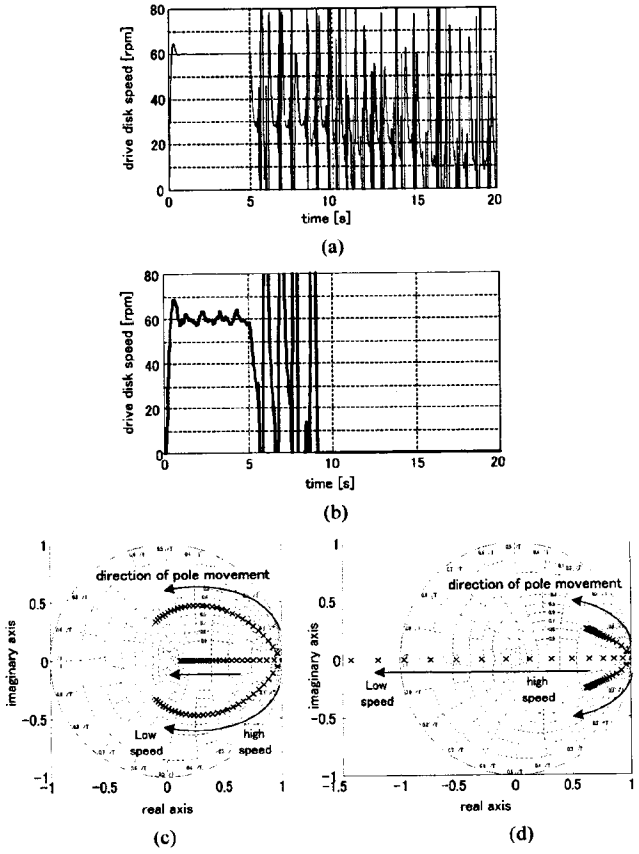

Fig. 4. (a) Simulation and (b) experimental results of the conventional pole assignment. (c) Movement of the poles in design. (d) Actual movement of the poles.

Equation (7) is very useful in pole assignment as it guarantees that the actual pole of the observer is placed as shown in Fig. 3(c) and (d). This maintains the stability of the system as shown in Fig. 3(a) and (b). An example when (7) is not used in pole placement is shown in Fig. 4. The observer gain is calculated by fixing the pole on s-plane and transform to z-plane by using T_1 as the sampling time. It is seen that an actual pole of the observer moves outward the unit circle, eventhough the poles moves inside the unit circle in the design. As a result, the control system cannot operate stably.

C. Comparison to the Conventional Method

T_1 is defined as the period between two consecutive pulses detected by the observer, so it is variable. When dealing with a variable-sampling-time system, the controller and the observer are conventionally designed by using T_1 as the sampling times. The conventional predicting observer equation is described by

$$\hat{\mathbf{x}}[m+1] = \mathbf{A}_1\hat{\mathbf{x}}[m] + \mathbf{B}_1\mathbf{u}[m] + \mathbf{L}_{1\mathrm{p}}(\mathbf{y}[m] - \mathbf{C}_1\hat{\mathbf{x}}[m]) \quad (8)$$

Note that subscript 1 indicates that T_1 is used as a sampling time. The observer gain is conventionally obtained as

$$\prod_{i=1}^{q}(z - z_i) = |z\mathbf{I} - (\mathbf{A}_1 - \mathbf{L}_{1\mathrm{p}}\mathbf{C}_1)|. \quad (9)$$

Using the fact that $\mathbf{A}_2^N = \mathbf{A}_1$ and $\mathbf{C}_2 = \mathbf{C}_1$, and comparing (9) and (7), the relation of the observer gain matrices of the dual-sampling-rate observer and the discrete-time observer, where T_1 is the sampling time given by

$$\mathbf{L}_{2\mathrm{p}}^* = \left(\mathbf{A}_2^{N-1}\right)^{-1}\mathbf{L}_{1\mathrm{p}} \quad (10)$$

where $\mathbf{A}_2^{N-1}$ is always nonsingular. By this fact, it is possible to calculate the observer gain of the dual-sampling-rate observer by the conventional method and then converting by (10) to stabilize the predicting dual-sampling-rate observer.

V. Current Dual-Sampling-Rate Observer

The other structure of the dual-sampling-rate observer can be derived based on the current observer [16], which utilizes the current measurement signal to correct the state variables at that instant. The signal and block diagrams are shown in Fig. 2(c) and (d), respectively. The algorithm of the current dual-sampling-rate observer is separated into state prediction and error correction as follows.

State prediction:

$$\tilde{\mathbf{x}}[n] = \mathbf{A}_2\hat{\mathbf{x}}[n-1] + \mathbf{B}_2\mathbf{u}[n-1], \quad n = 1, 2, \ldots, N, \quad (11)$$

TABLE III
COMPARISON OF PREDICTIVE- AND CURRENT DUAL-SAMPLING-RATE OBSERVER

	Predicting type	Current type
Algorithm	State prediction at $n=1,\cdots,N-1$ $\hat{\mathbf{x}}[n+1]=\mathbf{A}_2\hat{\mathbf{x}}[n]+\mathbf{B}_2\mathbf{u}[n]$ Error correction at $n=0$ $\hat{\mathbf{x}}[n+1]=\mathbf{A}_2\hat{\mathbf{x}}[n]+\mathbf{B}_2\mathbf{u}[n]+\mathbf{L}^*_{2p}\left(\mathbf{y}[n]-\mathbf{C}_2\hat{\mathbf{x}}[n]\right)$	State prediction at $n=1,\cdots,N$ $\hat{\mathbf{x}}[n]=\mathbf{A}_2\hat{\mathbf{x}}[n-1]+\mathbf{B}_2\mathbf{u}[n-1]$ Error correction: $n=N$ $\hat{\mathbf{x}}[n]=\mathbf{A}_2\hat{\mathbf{x}}[n-1]+\mathbf{B}_2\mathbf{u}[n-1]$ $+\mathbf{L}^*_{2c}\{\mathbf{y}[n]-\mathbf{C}_2(\mathbf{A}_2\hat{\mathbf{x}}[n-1]+\mathbf{B}_2\mathbf{u}[n-1])\}$
Observer gain	$\mathbf{L}^*_{2p}=\left(\mathbf{A}_2^{N-1}\right)^{-1}\mathbf{L}_{1p}$ where $\mathbf{L}_{1p}$ is the observer gain matrix of the predicting observer sampled by T_1 Gain recalculation is necessary	$\mathbf{L}^*_{2c}=\mathbf{L}_{1c}$ where $\mathbf{L}_{1c}$ is the observer gain matrix of the current observer sampled by T_1 Gain recalculation is unnecessary

Error correction:

$$\hat{\mathbf{x}}[n]=\begin{cases}\tilde{\mathbf{x}}[n] & n=1,2,\ldots,N-1\\ \tilde{\mathbf{x}}[n]-\mathbf{L}^*_{2c}(\mathbf{y}[n]-\mathbf{C}\tilde{x}[n]) & n=N\end{cases} \tag{12}$$

Note that the observer corrects the error only when $n=N$, i.e., at the instant when the measurement signal is detected. But we also define the "updating" process ($n=1,\ldots,N-1$ in (12)) as correction for simplicity. Equations (11) and (12) can be rearranged as shown (13) at the bottom of the page.

Rearranging (13) and analyzing in a fashion similar to that of (5) and (7), the observer gain matrix is obtained by placing the poles inside the unit circle and solving the equation

$$\prod_{i=1}^{q}(z-z_i)=\left|z\mathbf{I}-(\mathbf{A}_2^N-\mathbf{L}^*_{2c}\mathbf{C}_2\mathbf{A}_2^N)\right|. \tag{14}$$

Since $\mathbf{A}_2^N=\mathbf{A}_1$ and $\mathbf{C}_2=\mathbf{C}_1$, (14) becomes

$$\prod_{i=1}^{q}(z-z_i)=|z\mathbf{I}-(\mathbf{A}_1-\mathbf{L}^*_{2c}\mathbf{C}_1\mathbf{A}_1)|=0. \tag{15}$$

The observer gain, L_{1c}, of a conventional current observer sampled by T_1 is obtained by solving the equation

$$\prod_{i=1}^{q}(z-z_i)=|z\mathbf{I}-(\mathbf{A}_1-\mathbf{L}_{1c}\mathbf{C}_1\mathbf{A}_1)|=0. \tag{16}$$

Therefore, it can be concluded that the relation of the current dual-sampling-rate observer and the conventional current observer is given by

$$\mathbf{L}^*_{2c}=\mathbf{L}_{1c}. \tag{17}$$

The accurate gain matrix of the current dual-sampling-rate observer is, therefore, identical to that of the conventional current observer sampled by T_1. This simplifies the gain-tuning procedure since the observer gain matrix can be calculated by using the variable pulse interval T_1 as the sampling time without special gain conversion as the predicting type requires. The other advantage of the current dual-sampling-rate observer is that the corrected state variables are used to determine the control effort at that sampling instant, whereas those of the predicting dual-sampling-rate observer are used to determine the control effort in the next sampling. This theoretically improves the accuracy of the control system. Comparison of the predicting and current dual-sampling-rate observer is summarized in Table III.

VI. GAIN CALCULATING PROCEDURE

The gains of the observers can be simply calculated by consideration of the relationship of the observer gain matrices in (10) and (17). The gain calculating procedure is concluded as follows in two steps.

Step1: Placing the poles and calculating the observer gain matrix $\mathbf{L}_{1p}$ or $\mathbf{L}_{1c}$ by the conventional method.

Step2: Using the relationship in (10) or (17) to calculate the accurate observer gain matrix of the dual-sampling-rate observer $\mathbf{L}^*_{2p}$ or $\mathbf{L}^*_{2c}$.

The observer gain matrix of the predicting type $\mathbf{L}^*_{2p}$ varies according to N, which is the number of the intersampling, or the ratio of T_1 to T_2. In practice, we can easily apply this gain tuning by off-line calculation and storing the calculated gain matrix in a look-up table.

Step 2 can be omitted for the current type, in practice, since the gains are identical. Hence, it is not necessary to prepare the gain table in advance. This is the major advantage of the current type.

VII. SIMULATION AND EXPERIMENTAL VERIFICATION

The dual-sampling-rate observer and the proposed pole assignment have been verified by the experimental apparatus shown in Fig. 5. It is composed of an inertia-adjustable drive

$$\hat{\mathbf{x}}[n]=\begin{cases}\mathbf{A}_2\hat{\mathbf{x}}[n-1]+\mathbf{B}_2\mathbf{u}[n-1], & n=1,\cdots,N-1\\ \mathbf{A}_2\hat{\mathbf{x}}[n-1]+\mathbf{B}_2\mathbf{u}[n-1]+\mathbf{L}^*_{2c}\{\mathbf{y}[n]-\mathbf{C}_2(\mathbf{A}_2\hat{\mathbf{x}}[n-1]+\mathbf{B}_2\mathbf{u}[n-1])\} & n=N\end{cases} \tag{13}$$

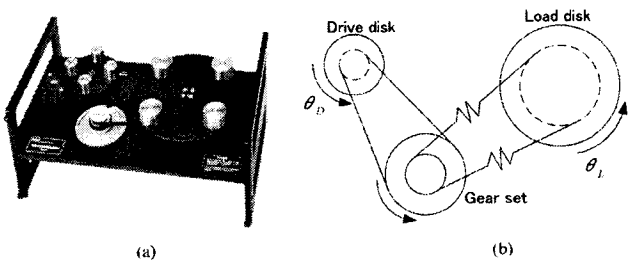

Fig. 5. (a) Experimental apparatus. (b) Free body diagram.

TABLE IV
LIST OF PARAMETERS

Symbol	Quantity	Value
c_D	Drive friction	0.004 Nm/rad/s
c_L	Load friction	0.05 Nm/rad/s
g_r	Gear ratio	4
J_D	Drive inertia and gear set inertia	0.00252 kgm^2
J_L	Load inertia	0.0271 kgm^2
K_{DL}	Flexible belt's equivalent torsional spring constant	8.45 Nm/rad

disk driven by a brushless dc motor and an inertia-adjustable load disk. Belts connect both disks to each other via a speed reduction gear set. 16 000-ppr rotary encoders are installed to measure the speed of each disk, but the resolution for the control is reduced to 80 ppr to verify the performance of the observer. The control period is set to 1.768 ms. List of the parameters and their values are shown in Table IV.

The objectives of the verification are:

1) to verify the effectiveness of the proposed pole assignment;
2) to compare the predicting and current dual-sampling rate-observer;
3) to examine the effect when the period between the pulse is nearly equal to control period (effect of small T_1/T_2 ratio);
4) to confirm the merit of the generalization in order to handle high-order plants.

A. Verification of the Proposed Pole Assignment Method

For simplicity, the proposed pole assignment method is verified based on a one-inertia system. The plant transfer function is described as

$$\frac{\omega_{\mathrm{D}}(s)}{T_{\mathrm{m}}(s)} = \frac{1}{J_{\mathrm{D}}s + c_{\mathrm{D}}} \tag{18}$$

where T_{m} denotes the motor torque. The controller is designed such that the equivalent time constant of the system is 200 ms. Consequently, the third-order observer is enough to estimate the whole state variables including disturbance. Its state equation is expressed in (3) for the predicting type and in (13) for the current type, where the state, input, and output vectors are described as

$$\hat{\mathbf{x}} = [\hat{\theta}_{\mathrm{D}} \quad \hat{\omega}_{\mathrm{D}} \quad \hat{T}_{\mathrm{L}}]^T, \quad \mathbf{u} = T_{\mathrm{m}}, \quad \hat{\mathbf{y}} = \hat{\theta}_{\mathrm{D}}. \tag{19}$$

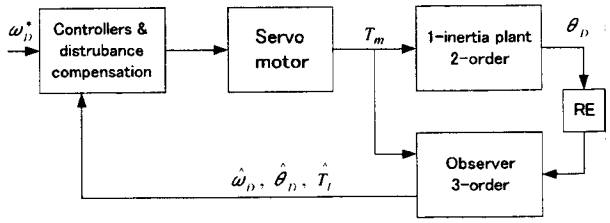

Fig. 6. Block diagram for verification of the pole assignment method.

where $\hat{\theta}_{\mathrm{D}}$, $\hat{\omega}_{\mathrm{D}}$, and $\hat{T}_L$ denotes the drive disk's angle, speed and the load torque. Coefficient matrices $\mathbf{A}_2, \mathbf{B}_2$, and $\mathbf{C}_2$ in (3) and (13) are derived from their continuous-time domain matrices with zeroth-order disturbance consideration $\mathbf{A}_{\mathrm{cd3}}, \mathbf{B}_{\mathrm{cd3}}$, and $\mathbf{C}_{\mathrm{cd3}}$, respectively. The subscript 3 means third order. The components of these matrices are described as

$$\mathbf{A}_{\mathrm{cd3}} = \begin{bmatrix} 0 & 1 & 0 \\ 0 & 0 & \frac{1}{J_{\mathrm{D}}} \\ 0 & 0 & 0 \end{bmatrix}, \quad \mathbf{B}_{\mathrm{cd3}} = \begin{bmatrix} 0 \\ \frac{1}{J_{\mathrm{D}}} \\ 0 \end{bmatrix},$$
$$\mathbf{C}_{\mathrm{cd3}} = [1 \quad 0 \quad 0]. \tag{20}$$

Note that the friction c_{D} in (18) is considered as a disturbance so it is not expressed in the state transition matrix in (20). Fig. 6 shows the block diagram of the controlled system.

It is important to note that the interval between two consecutive pulses produced from the rotary encoder changes according to speed. In many systems, where an ordinary discrete-time observer is implemented, the observer is conventionally designed at nominal operating speed by placing the poles on s-plane so that the desirable settling time is obtained and then mapping the poles on the s-plane to the z-plane by using the interval between the pulses T_1 as the sampling time [4]. In the case of a wide-speed-range system, the observer poles may be changed according to the speed in order to maintain the relationship between the time constant of the system and the observer. Note that the poles of the instantaneous speed observer, which are similar to the third order predicting dual-sampling-rate observer, was previously placed by this method.

The results and pole locations in the case when the poles of the observer are designed by the conventional method are shown in Fig. 4. The time constant of the observer is twice as fast as that of the system at any speed. However, the system cannot be stably driven when the speed drops below 60 r/min. This is because the poles are fixed on the s-plane and mapped to the z-plane without consideration of the relation of T_1 and T_2. Fig. 4(c) and (d) shows the movements of the observer poles in design and actual pole movements, respective. It is obviously seen in Fig. 4(d) that an actual pole of the observer moves onto the negative real axis when the speed drops below 53 r/min and proceeds to the outward direction of the unit circle. This confirms the fact that placing the poles without considering the relationship between the two sampling times causes instability. One way to solve this instability problem is to fix the poles on z-plane and reduce the controller gains to maintain the ratio of the time constant between the observer and the controlled system. But this will result in slow response of the system [9].

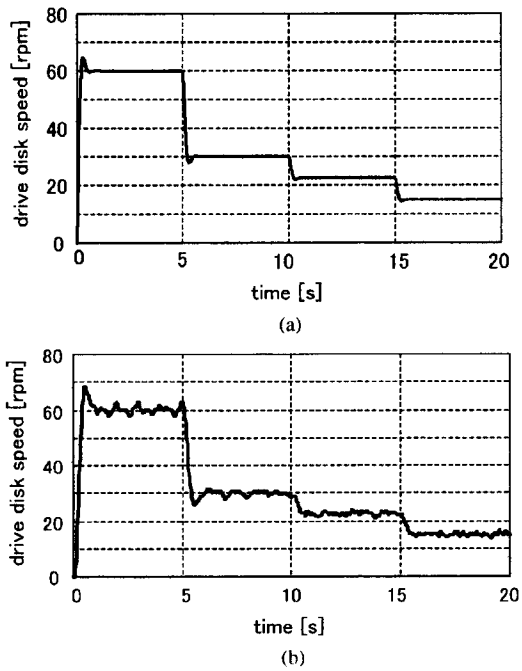

Fig. 7. (a) Simulation and (b) experimental results when the current dual-sampling-rate observer is applied.

Fig. 3 shows the results and pole locations by using the proposed pole assignment method. It is seen that by using the relation in (10) the gains are adjusted so that the poles move inside the unit circle on both z-planes, as shown in Fig. 3(c) and (d). Hence, the system can operate stably, as shown in Fig. 3(a) and (b). Note that the speed of 15 rpm corresponds to the pulse interval T_1 of 50 ms in case of the encoder's resolution of 80 ppr and the control period T_2 is set to 1.768 ms. In other words, T_1 is 28 times greater than T_2. This emphasizes the fact that the proposed pole assignment method maintains the stability and allows us to design a fast controller even at low speeds so that the desirable response can be achieved.

B. Comparison of the Predictive and Current Dual-Sampling-Rate Observers

The simulation and the experimental results in case of the current dual-sampling-rate observer are shown in Fig. 7. The observer gains are calculated based on the relation in (17), i.e., without special gain mapping that is necessary in the case of the predicting type. Then the system can stably operate as well as the predicting type shown in Fig. 3.

C. Effect of small T_1/T_2 ratio

Since the observer gains depend on the ratio between the error-correction period T_1 and the estimation period T_2 the observer gains are not continuous. This results in abrupt change of gains, especially at small T_1/T_2 ratios.

To examine this effect, the encoder resolution is increased to 1280 ppr, while the speed command is still the same as in Figs. 3, 4, and 7. The experimental results are shown in Fig. 8. Note that

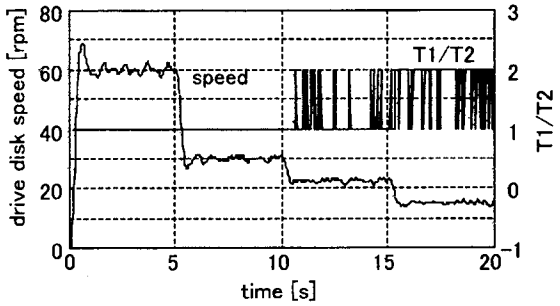

Fig. 8. Experimental result when T_1/T_2 ratio is small.

the commands of 60, 30, 22.5, and 15 r/min correspond to the T_{1_actual}/T_2 ratios of 0.442, 0.884, 1.18, and 1.77, respectively. According to the principle of the dual-sampling-rate observer, the T_1/T_2 ratios equals a value of 1 when the commands are 60 and 30 r/min. On the other hand, at the speed commands of 22.5 and 15 r/min the T_1/T_2 ratios are either 1 or 2. Hence, it is possible not only to examine the effect of T_1 / T_2 ratio, but also to verify that the dual-sampling-rate observer becomes an ordinary discrete-time observer, when the interval between the pulses is smaller than the control period. The results in Fig. 8 positively confirm that small T_1 / T_2 ratios do not yield result in undesirable effects to the system.

D. Confirmation of the Merits of Generalization

In this section, the merit of generalization is verified by applying the dual-sampling-rate observer to a two-inertia system. The experimental apparatus in Fig. 5 is set to obtain a two-inertia system. The frequency response of the plant is shown in Fig. 9. The plant state equation is described as

$$\dot{\mathbf{x}} = \mathbf{A}x + \mathbf{B}u, \qquad y = \mathbf{C}\mathbf{x} \tag{21}$$

where

$$\mathbf{A} = \begin{bmatrix} 0 & 1 & 0 & 0 \\ -\frac{k_{DL}}{g_r^2 J_D} & -\frac{c_D}{J_D} & \frac{k_{DL}}{g_r J_D} & 0 \\ 0 & 0 & 1 & 0 \\ \frac{k_{DL}}{g_r J_l} & 0 & -\frac{k_{DL}}{J_L} & -\frac{c_L}{g_r J_L} \end{bmatrix}$$

$$\mathbf{B} = \begin{bmatrix} 0 \\ \frac{1}{J_D} \\ 0 \\ 0 \end{bmatrix}, \quad \mathbf{C} = [0 \quad 1 \quad 0 \quad 0] \tag{22}$$

$$\mathbf{x} = [\theta_D \quad \omega_D \quad \theta_L \quad \omega_L]^T, \quad u = T_m, \quad y = \omega_D.$$

In case of the original instantaneous speed observer, it can estimate only the speed of the motor. Hence, it is impossible to control the whole state variables of the plant. This condition is emulated by using the dual-sampling-rate observer for one-inertia system that is designed by considering only the drive disk as the plant model. The structure of the observer is the same as described in (19) and (20). Let us define it as the "partial dual-sampling-rate observer." It is compared with the

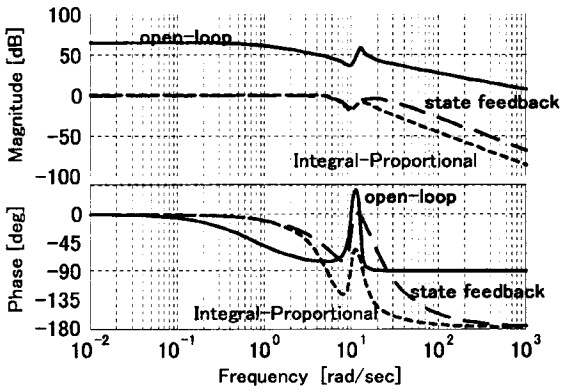

Fig. 9. Frequency response of the two-inertia plant.

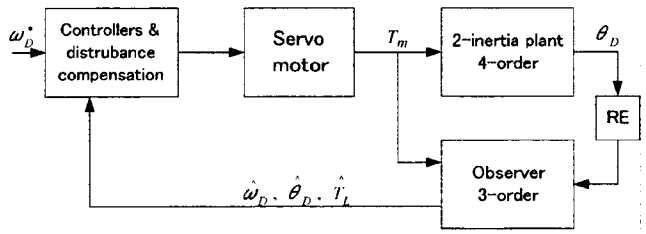

Fig. 10. Block diagram when the partial dual-sampling-rate observer is applied.

"full-state dual-sampling-rate observer," which is extended for the two-inertia system. Note that the predicting type is used in this experiment.

1) Partial Dual-Sampling-Rate Observer: The block diagram in this case is shown in Fig. 10. Since the partial dual-sampling-rate observer is applied, only the state variables of the drive disk can be estimated. As a result, an integral-proportional (IP) controller is designed. The predicting dual-sampling-rate observer and its corresponding pole assignment are applied. The simulation and the experimental results are shown in Fig. 11. It can be seen that the dynamics of the load disk causes oscillation compared to the case in Fig. 3(a) and (b).

2) Full-State Dual-Sampling-Rate Observer: An effective method to solve this problem is to design the controller by using state feedback. To do this, it is necessary to grasp all state variables. However, it is impossible to obtain the state variables directly because there is only one low-resolution rotary encoder installed at the drive disk. The full-state dual-sampling-rate observer is, therefore, introduced to the system. It can be implemented easily because it is written in state-space representation. The observer equation is as expressed in (3), where the state, input, and output vectors are described as follows:

$$\hat{\mathbf{x}} = [\hat{\theta}_{\mathrm{D}} \quad \hat{\omega}_{\mathrm{D}} \quad \hat{\theta}_{\mathrm{L}} \quad \hat{\omega}_{\mathrm{L}} \quad \hat{T}_{\mathrm{L}}]^T, \quad \mathbf{u} = T_{\mathrm{m}}, \quad \hat{y} = \hat{\theta}_{\mathrm{D}} \quad (23)$$

The list of the symbols are shown in Tables I and II. The matrices $\mathbf{A}_2, \mathbf{B}_2$, and $\mathbf{C}_2$ in (3) are derived from their continuous

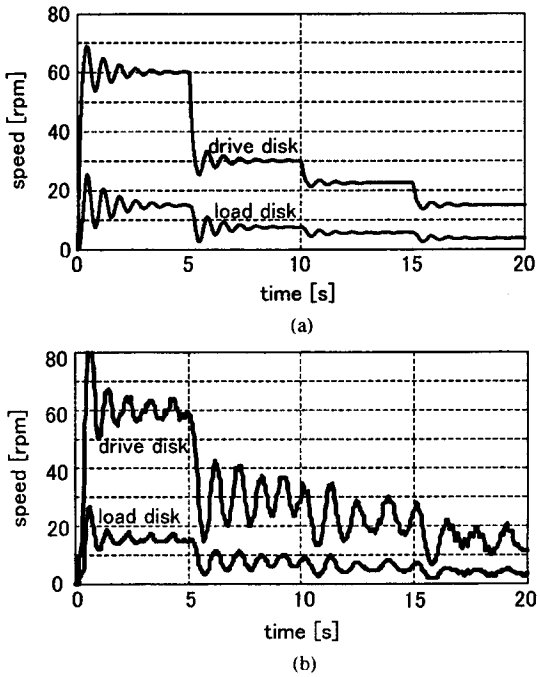

Fig. 11. (a) Simulation and (b) experimental results when the partial dual-sampling-rate observer is applied.

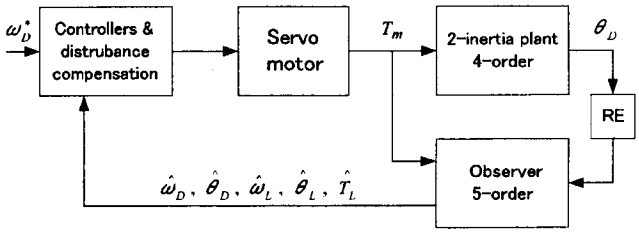

Fig. 12. Block diagram when the full-state dual-sampling-rate observer is applied.

time domain matrices with zero order disturbance consideration $\mathbf{A}_{\mathrm{cd5}}, \mathbf{B}_{\mathrm{cd5}}$, and $\mathbf{C}_{\mathrm{cd5}}$ respectively. The subscript 5 means fifth order. The components of these matrices are described as follows

$$\mathbf{A}_{\mathrm{cd5}} = \begin{bmatrix} 0 & 1 & 0 & 0 & 0 \\ -\frac{k_{\mathrm{DL}}}{g_{\mathrm{r}}^2 J_{\mathrm{D}}} & -\frac{c_{\mathrm{D}}}{J_{\mathrm{D}}} & \frac{k_{\mathrm{DL}}}{g_{\mathrm{r}} J_{\mathrm{D}}} & 0 & \frac{1}{J_{\mathrm{D}}} \\ 0 & 0 & 0 & 1 & 0 \\ \frac{k_{\mathrm{DL}}}{g_{\mathrm{r}} J_{\mathrm{L}}} & 0 & -\frac{k_{\mathrm{DL}}}{J_{\mathrm{L}}} & -\frac{c_{\mathrm{L}}}{J_{\mathrm{L}}} & 0 \\ 0 & 0 & 0 & 0 & 0 \end{bmatrix}$$

$$\mathbf{B}_{\mathrm{cd5}} = \begin{bmatrix} 0 \\ \frac{1}{J_{\mathrm{D}}} \\ 0 \\ 0 \\ 0 \end{bmatrix}, \quad \mathbf{C}_{\mathrm{cd5}} = [1 \quad 0 \quad 0 \quad 0 \quad 0]. \quad (24)$$

The block diagram is shown in Fig. 12. Since the observer can estimate the state variables of both disks, a state feedback controller can be designed. The controller gains are adjusted in order to obtain the system's equivalent time constant of 200 ms.

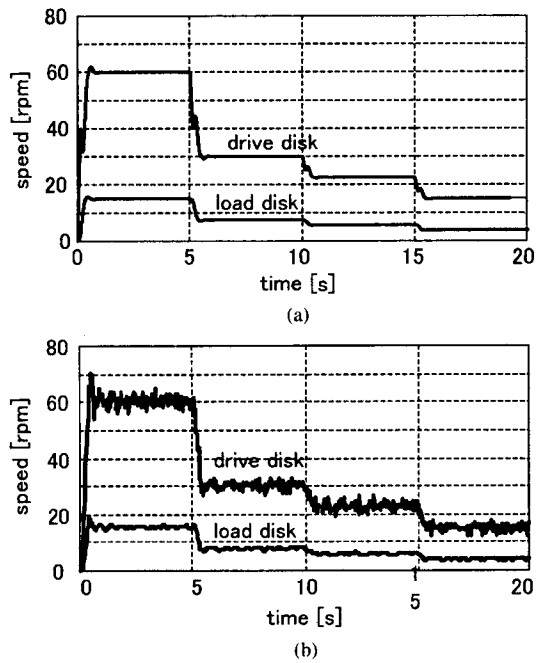

Fig. 13. (a) Simulation and (b) experimental results when the full-state dual-sampling-rate observer is applied.

Like the previous case, where the partial observer has been applied, the observer time constant is set to 50 ms. The simulation and the experimental results are shown in Fig. 13. Since the whole state variables are available and the state feedback controller can be implemented, the oscillation can be remarkably suppressed compared to the results in Fig. 11. This confirms the merit of the generalization that allows us to design a high-order observer for state feedback controller design.

VIII. Conclusion

This paper describes by introducing dual-sampling-rate observer, an effective way to achieve precise intersampling estimation from an event-based sampling system such as traction control, in which a low-resolution encoder are commonly used as the speed sensors. Its principle is to estimate or predict the state variables between the encoder pulses based on model-based knowledge of physical plant dynamics and correct the estimation error when the next encoder pulse is generated. It is classified into two types based on its structure: the predicting type and the current type. It can be extended for estimating a high-order plant easily, since it has been generalized in state space representation. This extension has allowed us to estimate the whole state variables. This has made the design of state feedback possible, and the control performance was improved from that of the conventional methods.

The observer has two sampling times: the constant period of estimation T_2 equal to the control period and the variable period of error correction T_1 equal to the pulse interval detected by the observer. This has lead to the proposal of a novel pole placement method that stabilizes the operation of the observer in all speed range by considering the relationship between T_1 and T_2. We have also found the relationship between the observer gains of the dual-sampling-rate observer and the variable-sampling-single-rate observer, sampled by T_1. This relationship has simplified the gain calculating procedure, especially in the case of the current type where the observer gain is identical to the variable-sampling-single-rate observer, sampled by T_1.

The effectiveness of the proposed observer has been verified through various simulations and experiments based on a two-inertia system. The results have confirmed that it can operate stably, especially at low speed, and can be applied to not only a motor but also any high-order plants.

References

[1] R. D. Lorenz, "Microprocessor control of motor drive and power converters," *Microprocessor Motion Control of AC and DC Drive, IEEE Tutorial Course Note Book from 1991, 1992 and 1993, IEEE, IAS Annual Meetings*, IEEE Publishing Services #THO587-6.

[2] T. Ohmae, T. Matsuda, K. Kamiyama, and M. Tachikawa, "A microprocessor-controlled high-accuracy wide-range speed regulator for motor drives," *IEEE Trans. Ind. Electron.*, vol. IE-29, no. 3, pp. 207–221, Aug. 1982.

[3] Y. Hori, "Robust motion control based on a two-degrees-of-freedom servosystem," *Adv. Robot.*, vol. 7, no. 6, pp. 525–546, 1993.

[4] S. Sakai and Y. Hori, "Ultra-low speed control of servomotor using low resolution rotary encoder," in *Proc. 1995 IEEE IECON 21st Int. Conf. Ind. Electron., Control, Instrum.*, Orlando, FL, Nov. 1995, vol. 1, pp. 615–620.

[5] G. Guidi, H. Kubota, and Y. Hori, "Induction motor control for electric vehicle application using low resolution position sensor and sensorless vector control technique," in *Proc. Power Convers. Conf.*, Nagaoka, Japan, 1997, pp. 937–942.

[6] S. Lee, T. Lasky, and S. Velinsky, "Improved velocity estimation for low-speed and transient regimes using low-resolution encoders," *IEEE/ASME Trans. Mechatronics*, vol. 9, no. 3, pp. 553–560, Sep. 2004.

[7] M. Cao, K. Takeuchi, T. Furuya, and A. Kawamura, "Adhesion control in low-speed region and experiment verification with considering low-resolution pulse generator," in *Proc. Power Convers. Conf.*, Osaka, Japan, 2002, pp. 873–878.

[8] L. Kovudhikulrungsri and T. Koseki, "Speed estimation of induction motor in low speed for pure electric brake," in *Proc. Transp. Electr. Railways Linear Drive Conf.*, Sapporo, Japan, Jul. 2000, pp. 19–24.

[9] ——, "Control of an induction motor for pure electric brakes," in *Proc. 2001 Jpn. Ind. Appl. Soc. Conf.*, Matsue, Japan, Aug. 2001, vol. 3, pp. 1297–1303.

[10] ——, "Precise speed and torque control for AC traction pure electric braking system in low speed range," *Trans. Inst. Electr. Eng. Jpn.*, vol. 122-D, no. 11, pp. 1027–1033, 2002.

[11] M. Araki and T. Hagiwara, "Multivariable multirate sampled-data system: state-space description, transfer characteristics and Nyquist criterion," *IEEE Trans. Autom. Control*, vol. AC-31, no. 2, pp. 145–154, Feb. 1986.

[12] M. Araki and K. Yamamoto, "Pole assignment by multirate sampled-data output feedback," *Int. J. Control*, vol. 44, no. 6, pp. 1661–1673, 1986.

[13] H. M. Al-Rahmani and G. F. Franklin, "Multirate control: A new approach," *Automatica*, vol. 28, no. 1, pp. 35–44, 1992.

[14] H. Fujimoto and Y. Hori, "High performance servo systems based on multirate sampling control," *Int. Fed. Autom. Control J. Control Eng. Practice*, vol. 10, no. 7, pp. 773–781, 2002.

[15] L. Kovudhikulrungsri and T. Koseki, "Improvement of performance and stability of a drive system with a low-resolution position sensor by multirate sampling observer," *Trans. Inst. Elect. Eng. Jpn.*, vol. 124-D, no. 9, pp. 886–892, 2004.

[16] A. Tewari, *Modern Control Design with MATLAB and SIMULINK*. New York: Wiley, 2002.

Lilit Kovudhikulrungsri (S'01–M'04) received the Ph.D. degree in electrical engineering from the University of Tokyo, Tokyo, Japan, in 2004.

He is currently with Nippon Seiko Kabushiki Kaisha (NSK Ltd.), Tokyo, Japan. His current research interests include steering systems, control systems, and electric drives.

Takafumi Koseki (S'87–M'92) received the Ph.D. degree in electrical engineering from the University of Tokyo, Tokyo, Japan, in 1992.

He is currently an Associate Professor in the Department of Information and Communication, University of Tokyo. His current research interests include applications of electrical engineering to public transport systems, especially to linear drives, and analysis and control of traction systems.

Dr. Koseki is a member of the Institute of Electrical Engineers of Japan, the Japan Society of Mechanical Engineering, the Japan Society of Applied Electromagnetics, and Mechanics, and Verein Deutscher Ingenieure.